Simulation of the development of small-angle X-ray scattering during the crystallization of polymers*

R. Vignaud and J. M. Schultz
Materials and Metallurgy Program, University of Delaware, Newark, DE 19716, USA
(Received 29 October 1984; revised 3 April 1985)

Small-angle X-ray scattering (SAXS) from one-dimensional transforming systems has been simulated. In order to show two limiting types of transformation behaviour, both 'classical' growth and the spinodal demixing of chain conformation defects have been modelled. Nests of simulated SAXS curves represent stages in the transformation process. It is shown that the following behaviour can be used to characterize the type of transformation: (a) motion of the SAXS peak position, (b) peak shape change, (c) second-order peak intensity, (d) intensity cross-over, and (e) intensity decrease.

(Keywords: small-angle X-ray scattering; crystallization; transformation behaviour; chain defects)

INTRODUCTION

An area of long-standing interest and importance in polymer science is the development of microstructure in semicrystalline polymers. A clear understanding of the processes involved provides the basis for the rationalization of industrial solidification and heat-treatment stages.

For some time it has been possible to characterize the development of overall crystallinity and of spherulites. In these cases, instruments for rapid data collection have long been available. On the other hand, *in situ* measurement of the development of crystallite colonies is relatively recent, since rapid measurement awaited new methodologies.

Specifically, microstructure at the crystallite lamellae level can be characterized by electron microscopy or by small-angle X-ray scattering (SAXS). Electron microscopy is inherently limited in its ability to follow microstructural change directly, since the specimen is damaged by the electron beam. SAXS produces no specimen deterioration, but until approximately ten years ago was restricted to *in situ* measurement of only very slow processes[1-4]. The introduction of position-sensitive detectors and synchrotron X-ray sources has dramatically reduced the time needed to obtain SAXS data and has thereby made *in situ* SAXS (ISSAXS) measurements of microstructural rearrangements possible.

ISSAXS measurements almost trivially yield long spacing data, but can also yield complete SAXS intensity maps. Similar results are also reported for materials crystallizing isothermally and then quenched to retain the structure present at the crystallization temperature, SAXS data being acquired later at room temperature. Such intensity maps or curves have been reported for the quiescent melt-crystallization of linear polyethylene[5,6], poly(ethylene terephthalate)[7], a poly(ethylene oxide)/polystyrene/poly(ethylene oxide) triblock copolymer[5], and poly(tetramethyl-*p*-silphenylene siloxane)[8] (TMPS); for the crystallization of stretched melts of polypropylene[9,10], lightly crosslinked polyisoprene[11], and poly(ethylene terephthalate)[12-14]; and of the recrystallization of cold-drawn polypropylene[15] and nylon-6,6.[16]

The evolution of SAXS intensity curves during a microstructural transformation embodies a great deal of information regarding the microstructural development itself. However, only infrequently has use been made of the details of the scattering curves. In the present work, simulated scattering curves for somewhat idealized crystallization processes are presented. Such nests of curves provide qualitative insights into the types of processes which are involved in the crystallization process. The goal of this simulation study is to provide the experimenter with nests of SAXS curves against which he may qualitatively compare his data.

Of particular interest has been the proposition that, under certain conditions of crystallization under strain, crystallization may progress by the spinodal demixing of chain defects[4,9,10,14,15,17]. In spinodal demixing, there are no sharp phase boundaries; rather, a continuously and periodically modulated density distribution increases in amplitude with time, until the peak density approaches that of the crystal phase and the trough density approaches that of the melt or glass. Such a process is in sharp contrast to classical nucleation and growth, which is known to prevail in slow, quiescent crystallization. In classical processes, the newly-formed crystalline regions immediately assume the equilibrium phase properties (to a first approximation) and the boundary between host melt (or glass) and crystal is sharp. Transformation progresses by the conversion of more melt to crystal, the motion of the crystal/melt boundary into the melt or by the creation of new crystallites. The detailed differences between these two potential modes of transformation should appear as detailed differences in the distribution of SAXS intensity in reciprocal space.

* Work supported by the National Science Foundation under Grant No. CPE 8303058.

0032-3861/86/050651-08$03.00

In the following two sections are described simulations of spinodal and of classical growth processes, respectively. The simulations are for relatively ideal cases, in one dimension. While an analytical simplification, the one-dimensionality applies directly to transformations in highly strained systems and to Lorentz-corrected results in spherulitic (spherically symmetric) systems. In the final section, some generalizations arising from the simulations are brought together.

MODELS AND SIMULATIONS

Case 1: Spinodal decomposition

Spinodal decomposition refers to the continuous demixing of a multicomponent system. One envisages the creation of a system in which the composition is represented by a continuous, periodic distribution of the components. This distribution can be described by a Fourier series or integral of standing composition waves of amplitudes $A(\underline{s})$, where $\underline{s}$ is the wave number of a given Fourier component. As demixing continues, some Fourier components grow in amplitude, while others shrink. The kinetics of this situation have been analysed by Cahn[18,19], Swanger *et al.*[20], de Fontaine[21], Cook[22] and Williams[23].

Cahn's linearized analysis results in the following rate expression for the amplitude:

$$A(\underline{s},t)=A(\underline{s},0)\exp[R(\underline{s})t] \tag{1}$$

Here $R(\underline{s})$, the amplification factor, depends on the interdiffusion coefficient $\tilde{D}$, on the second derivative of the Helmholtz free energy f of the system with respect to composition c_B, and on various material constants via

$$R(\underline{s})=4\pi s^2\tilde{D}\left[1+\frac{2\eta^2 Y}{(\partial^2 f/\partial^2 c_B^2)}+\frac{8\pi^2 K s^2}{(\partial^2 f/\partial c_B^2)}\right] \tag{2}$$

where η is the linear strain per unit composition difference, $Y=E/(1-\nu)$ for an isotropic solid in which E is Young's modulus and ν is Poisson's ratio, and K is the 'gradient energy coefficient'. The second term on the right of equation (2) represents coherency strains; the third term represents an incipient interfacial energy.

With respect to polymer crystallization, one envisages a chain which will become part of an existing crystal. Those repeat units which are already oriented parallel to the chain axis of the crystal constitute one component. Repeat units of any other orientation are the other component. In such a model the non-parallel, or defective, units may migrate along the chain. An end state would be attained when most defects accumulate in a melt-like region and most non-defective units align in crystalline registry. The early stages of transformation could proceed by spinodal decomposition.

The intensity of scattering at time t from a system undergoing spinodal decomposition is given by[18,19]

$$I(s,t)=I(s,o)\exp[2R(\underline{s})t] \tag{3}$$

It can be seen from equations (2) and (3) that $R(\underline{s})$, and consequently, $I(s,t)$, is always a peaked function in the spinodal region. $R(\underline{s})$ has zeros at $s=0$ and $s_c=-[(\partial^2 f/\partial c_B^2+2\eta^2 Y]^{1/2}/(2(2\pi)^{\frac{1}{2}}K^{\frac{1}{2}})$. Between these zeros $R(s)$ has its maximum at

$$s_{max}=\frac{1}{4\pi\sqrt{K}}\left(\frac{\partial^2 f}{\partial c_B^2}\right)+2\eta^2 Y \tag{4}$$

We note that $s_c=\sqrt{2}s_{max}$. At all $s>s_c$, $R(\underline{s})<0$ and the intensity decreases.

In equation (3), $I(s,0)$ is the scattered intensity due to the initial configuration of the system. For a random mix of components,

$$I(s,0)=\langle|f_n^2|\rangle-|\langle f_n\rangle|^2 \tag{5}$$

where f_n is the scattering amplitude from one isolated structural unit and the carets denote spatial averaging. $I(s,0)$ for random mixing is nearly constant over the small-angle regime. In the computations to be described here $I(s,0)$ is taken as an arbitrary scaling constant I_0.

The development of SAXS curves during spinodal decomposition was simulated using equations (2) and (3). We note that equation (3) can be simplified to

$$I(\underline{s},t)=C_1\exp[C_2 s^2(1-C_3 s^2)t] \tag{6}$$

Here C_1, C_2 and C_3 are scaling constants. The constant C_3 controls the position of the scattering peak and has been adjusted here to produce a peak representing a periodicity of 100 Å. In order to follow the course of scattering curve development, the values assigned to the scaling constants are unimportant, provided that the time t is carried through a broad range. In the present computations, the following constant values were used: $C_1=1$, $C_2=300$ Å^2 s^{-1}, $C_3=5000$ Å^2.

Figure 1 is a set of computed SAXS curves for linearized spinodal decomposition. The associated kinetics of development of the intensity at the maximum is shown in *Figure 2*.

The required $exp(At)$ kinetics are apparent. Physically, at longer times the intensity must slowly approach an asymptote; however the transition to this behaviour has not been explored here. It is useful to observe, in *Figure 1*, that the SAXS curves become narrower with increasing time; for spinodal decomposition, the curves are not self-similar. As an example, shown in *Figure 3* are curves for $t=10$ and $t=100$. Shown also is the $t=10$ curve with the

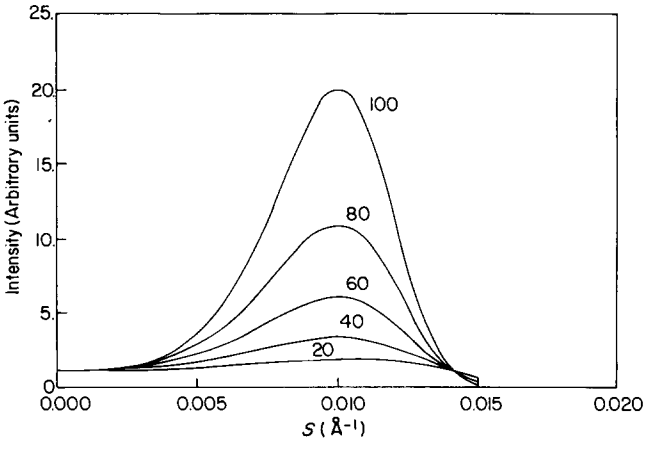

Figure 1 Simulated SAXS curves for spinodal demixing of chain conformational defects. Curves are shown for equally spaced time steps (seconds)

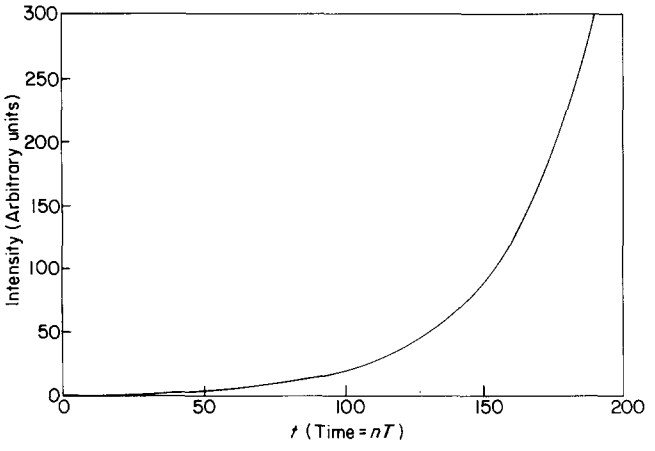

Figure 2 Kinetics of development of the simulated SAXS maximum

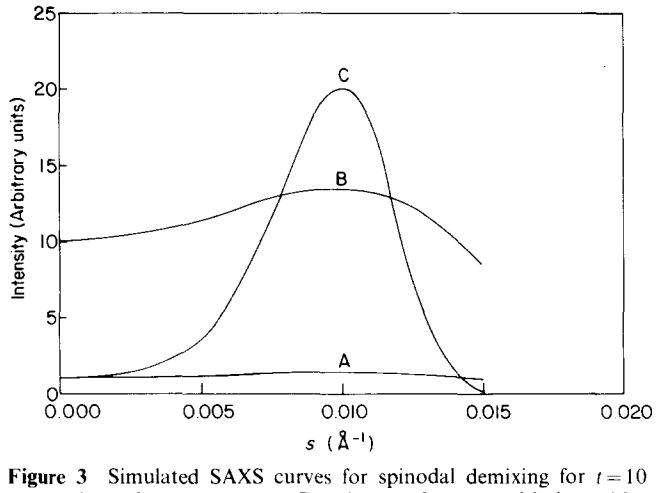

Figure 3 Simulated SAXS curves for spinodal demixing for $t=10$ (curve A) and $t=100$ (curve C). The $t=10$ curve with intensities multiplied by 10 is curve B

intensity multiplied by a factor of ten in order to bring the $t=10$ and $t=100$ curves to comparable intensities. The absence of self-similarity is apparent.

In some experimental studies of SAXS curve development during transformation, the scattering curve for $t=0$ is taken as the 'background' curve and is subtracted from curves at all $t>0$. If the $t=0$ curve is subtracted in this way from each of the curves of *Figure 1*, the result is as shown in *Figure 4*. The curves of *Figure 4*, unlike those of *Figure 1*, are self-similar. Furthermore, the intensity function at sufficiently small times can be written

$$I(s,t)-I(s,0)\simeq I(s,0)[2R(s)t] \tag{7}$$

This function is a straight line through the origin.

A final comment on scattering curves for spinodal decomposition relates to their shape. If the reciprocal space variable is taken as s^2, rather than s, the curve shape is gaussian. This is seen by replacing s in equation (6) by $b^{1/2}$. This replacement gives

$$I(s,t)=C_4 I(s,0)\exp[-(C_5 b-C_6)t] \tag{8}$$

where

$$C_4=\exp(C_6^2 t)$$
$$C_5^2=C_2C_3$$
$$C_6^2=C_2/4C_3$$

Equation (8) is a gaussian, offset from the origin. *Figure 5* shows the intensity at $t=100$ plotted against s^2 rather than against s. The gaussian shape is obvious.

Case 2: Classical growth

In this case, the intent is to provide a somewhat idealized model of the crystallization of spherulites[24,25] or of row structures[26,27] from the melt or the glass. For both spherulites and row structures, nucleation events are followed by the growth of crystallites from the nucleating sites. A two-phase lamellar structure develops directly from the melt or glass. As depicted in *Figure 6*, stacks of lamelliform crystals grow from the nucleating centre, through the addition of lamellae to the stack (*Figure 6a*) and also by the lateral growth of the crystalline lamellae (*Figure 6b*). The crystallites are separated from each other by amorphous layers. The process of nucleation and stack

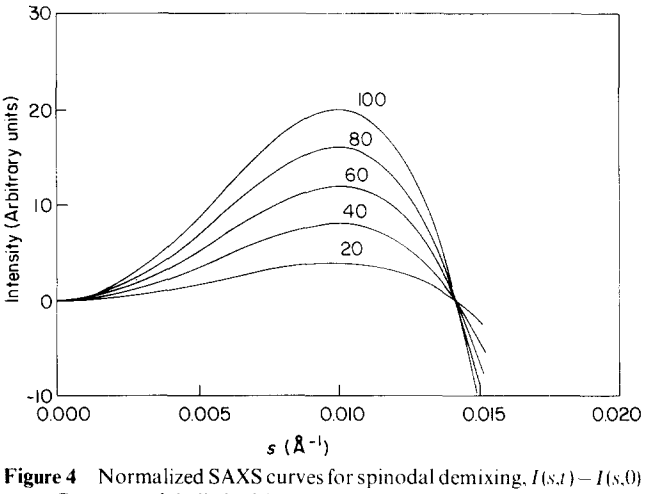

Figure 4 Normalized SAXS curves for spinodal demixing, $I(s,t)-I(s,0)$ vs. s. Curves are labelled with values of t (seconds)

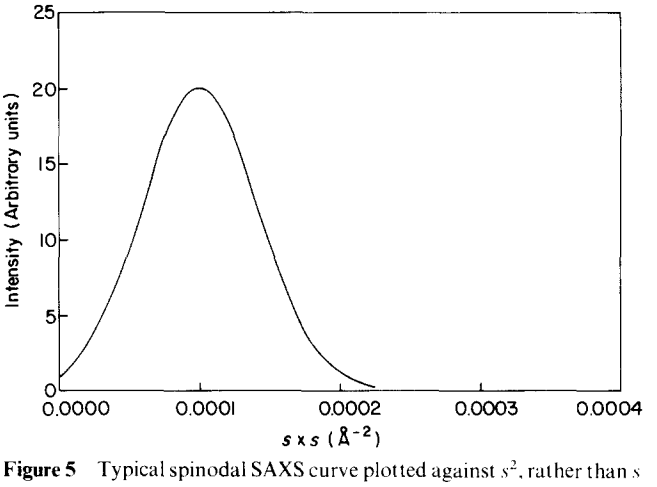

Figure 5 Typical spinodal SAXS curve plotted against s^2, rather than s

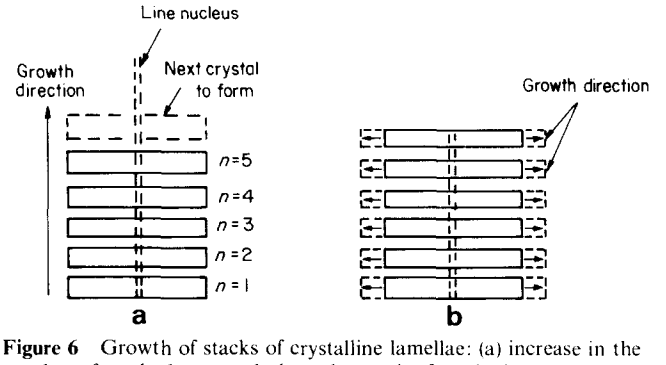

Figure 6 Growth of stacks of crystalline lamellae: (a) increase in the number of stack elements, (b) lateral growth of stack elements

extension is termed 'primary crystallization'. The as-formed crystallites and amorphous material are taken to be in the equilibrium state of the crystal and melt (or glass) phases. In addition, lamellae which have already formed thicken at the expense of the amorphous matter[28-31]. This process is termed 'secondary crystallization'. In the case of spherulitic growth from a quiescent melt or glass, many internally coherent stacks develop radially from one nucleating centre. A lateral direction of the lamellar crystallites is oriented radially. For row structures, the stacking direction is constant for all stacks in the material. The above model is broadly in line with what is known about the crystallization of polymers from the melt.

The nucleation events are to some extent distributed in time and space. The degree to which extrinsic or intrinsic heterogeneities are available as heterogeneous nucleation sites and the degree to which each heterogeneity is effective control the distribution of nucleated sites. While a general model for polymer crystallization must take account of the temporal distribution of nuclei, it has been assumed in the present work that all stacks within the material nucleate at time zero. This assumption is consistent with SAXS results on the crystallization of stretched rubber[32] and of poly(ethylene terephthalate)[33] from the highly-stretched melt. For crystallization from the quiescent melt, it would be necessary to include the distribution of nucleation times into the analysis. Thus the present simulation should be reasonably valid for stress-assisted crystallization, but would be only broadly indicative of what would happen in the spherulitic case.

Several more specific assumptions have been made. The assumptions relate finally to the computation of the scattered intensity $I(s,t)$. In general, the scattered intensity is the sum of two terms, I_1 and I_2, which are respectively the Bragg scattering due to the periodicity within the stack and the diffuse scattering due to variations of lamellar thickness within the stack. The periodic term can be written

$$I_1(s,t,) = F^2(s,t)Z(s,t) \tag{9}$$

where s, the scattering parameter, is $2\sin\theta/\lambda$; F, the 'structure factor', represents the scattering amplitude of one isolated repeat unit (one crystallite); and $Z(s,t)$, the lattice factor, represents the quasiperiodic distribution of crystallites in one-dimension. The assumptions are as follows.

(1) The one-dimensional stack of parallel crystallites is basically periodic, but the intercrystalline distances are distributed in a paracrystalline[34] manner. The degree of disorder is characterized by a parameter g, which is a measure of the width of an assumed gaussian distribution of intercrystallite distances $L(n)$ about the average value $\bar{L}$, g increasing with the breadth of that distribution. This assumption results, for a stack on N crystallites, in a lattice factor of the form[35],

$$Z_N(s) = 1 + 2\sum_{m=1}^{N}(1 - m/N)\rho^m \cos(2\pi m s\bar{L}) \tag{10}$$

where

$$\rho = \exp(-2g^2\pi^2\bar{L}^2s^2) \tag{11}$$

For very long stacks ($N \to \infty$), the lattice factor becomes

$$Z_N(s) = (1-\rho^2)/[1 + \rho^2 - 2\rho\cos(2\pi s\bar{L})] \tag{12}$$

It should be noted that in the above equations the time is characterized by the number N of crystallites instantaneously in the stack.

(2) The stack growth rate is constant in time, a new crystallite forming every T seconds. Since this growth is regular, the number N of crystallites can also be used as an index of the transformation time.

(3) Crystals thicken according to a logarithmic time law. For the nth crystallite in a stack,

$$L_n = L_0 + L_1 f(t,n) \tag{13}$$

where L_0 is the initial crystallite thickness, L_1 a parameter which scales the rate of crystal thickening, and

$$\begin{aligned} f(t,n) &= \log(t/nT) \quad \text{for } t > nT \\ f(t,n) &= 0 \qquad\qquad \text{for } t < nT \end{aligned} \tag{14}$$

(4) Stack extension (primary crystallization) and crystal thickening occur simultaneously, each crystal beginning to thicken as soon as it forms, as indicated in equation (14).

(5) Although the thickest crystals in a stack are those which formed first and the thinnest those which formed most recently, it is taken, for computational simplicity that the crystals of various thickness are randomly arranged in the stack. This simplification allows the diffuse scattering I_2 to be written,

$$I_2 = N\langle|F_n|^2\rangle - N|\langle F_n\rangle|^2 \tag{15}$$

where the carets denote averaging over all elements of the stack.

Using all of the above, the scattered intensity can now be computed according to

$$I(s,t) = |\langle F_n\rangle|^2 Z_N(s) + N\langle|F_n|^2\rangle - N|\langle F_n\rangle|^2 \tag{16}$$

In equations (15) and (16), the structure factor F_n is the scattering from the nth plate and is written

$$F_n(s,t) = \Delta\rho\{\sin[\pi s L_n(t)]\}/\pi s$$

Simulations were carried out under four conditions of initial lamellar thickness and rate of thickening. The periodicity of stacking is maintained constant at $\bar{L} = 100$ Å. Initial crystallite thicknesses L_0 used are 50 Å and 20 Å. For $L_0 = 50$ Å, the thickening rate scale parameter L_1 was assigned values of 10 Å and 1 Å. For $L_0 = 20$ Å, thickening rate scale parameters of 20 Å and 2 Å were used. In both cases, the transformation was allowed to proceed until $N = 100$.

Figure 7 shows the simulated transformation for $L_0 = 50$ Å, $L_1 = 10$ Å at times from T to $5T$ (*Figure 7a*) and $20T$ to $100T$ (*Figure 7b*). The results for the simulated transformation for $L_0 = 50$ Å, and $L_1 = 1$ Å (a slower thickening rate) are qualitatively very similar to *Figure 7* and are not shown. For $L_0 = 50$ Å, a SAXS Bragg peak builds quickly from an initial curve of continuously decreasing intensity (the square of the single platelet scattering factor). At early stages, the Bragg peak moves gradually toward larger angle, as the continuous scattering background vanishes. Thereafter, the peak position is sensibly constant. The change of peak position with transformation time is shown in *Figure 8* for

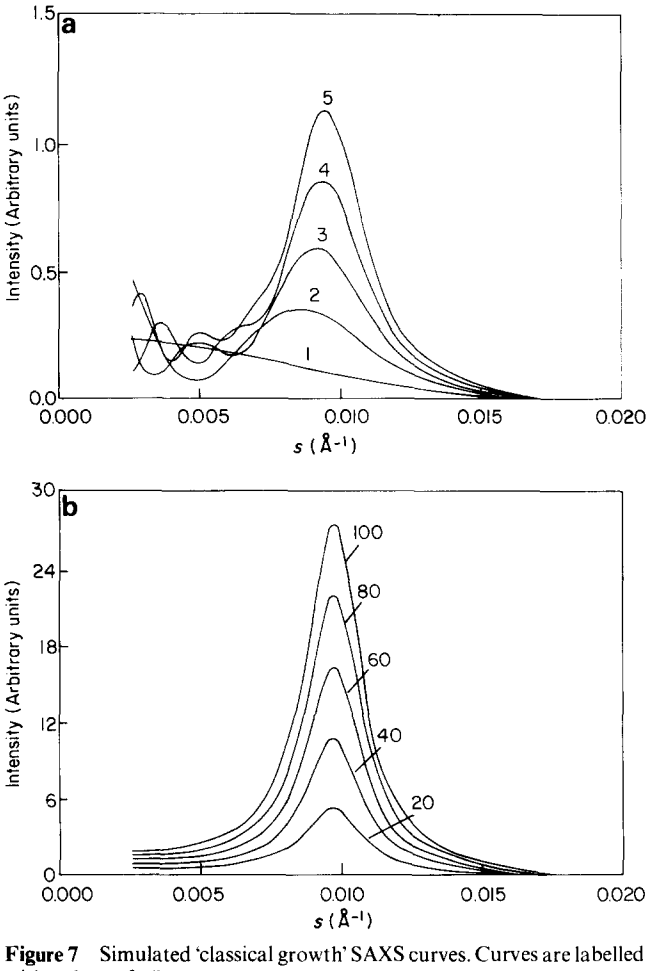

Figure 7 Simulated 'classical growth' SAXS curves. Curves are labelled with values of t/T

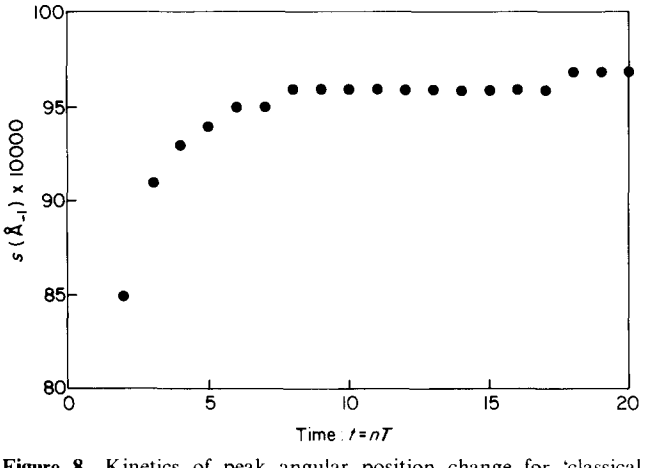

Figure 8 Kinetics of peak angular position change for 'classical growth', $L_0 = 50$ Å, $L_1 = 10$ Å

$L_0 = 50$ Å, $L_1 = 10$ Å. The change of intensity with transformation time for $L_0 = 50$ Å is shown in *Figure 9*. Up to the time at which stack-building is complete ($T = 100$), the intensity builds similarly for $L_1 = 1$ Å and $L_1 = 10$ Å. However, after $T = 100$, the intensity drops rapidly for the case of rapid secondary crystallization ($L_1 = 10$ Å), but immeasurably for $L_1 = 1$ Å. The decrease of intensity at the first order maximum when the complete stack is formed reflects the property that the structure factor at that point, $F_n(1/\bar{L},t)$ exhibits a maximum at $L_n(t)$ $0.5\bar{L}$, which was the initial thickness considered. At the same time the structure factor at the $2d$ order maximum, $F_n(2/\bar{L},t)$ is zero if $L_n(t) = 0.5\bar{L}$ and increases for higher $L_n(t)$. At that point, $F_n(s,t)$ is reduced to $F_n(2/\bar{L},t) = \Delta\rho\bar{L}(\sin(2\pi)/2\pi) = 0$. The presence or absence of a $2d$ order maximum is governed by the structure factor and the average degree of crystallinity. This is particularly obvious in the simulated SAXS curves for longer lines, corresponding to the first case ($L_0 = 50$ Å, $L_1 = 10$ Å) and shown in *Figure 10*; the first order peak decreases while the second order grows.

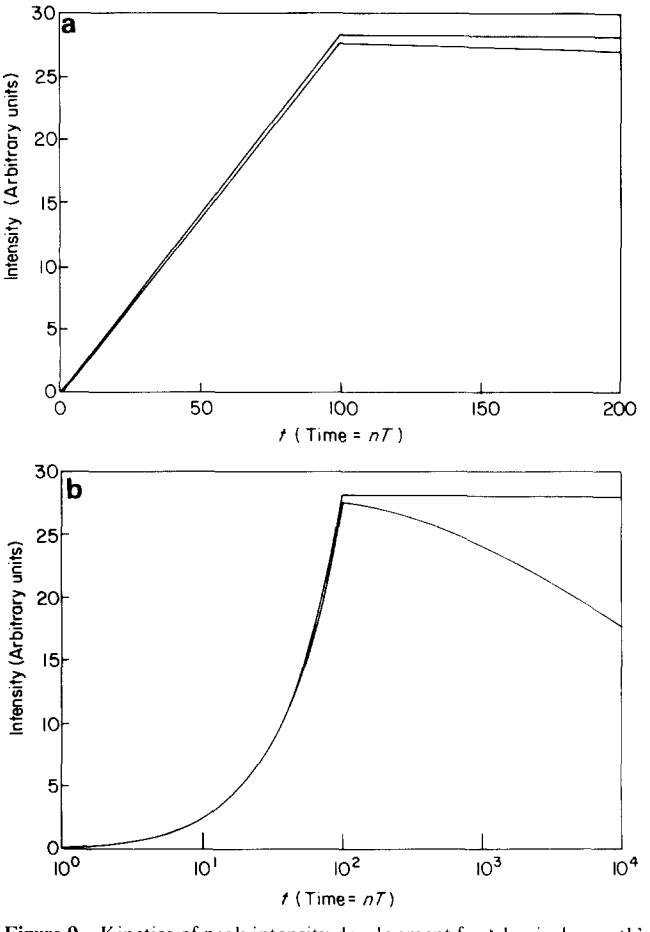

Figure 9 Kinetics of peak intensity development for 'classical growth' with $L_0 = 50$ Å and $L_1 = 1$ Å (upper curve) and $L = 10$ Å (lower curve): (a) linear time axis, (b) logarithmic time axis

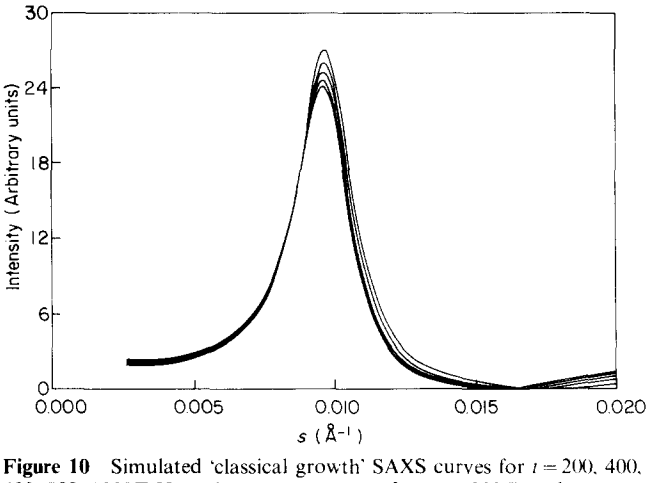

Figure 10 Simulated 'classical growth' SAXS curves for $t = 200$, 400, 600, 800, $1000T$. Here the curves progress from $t = 200T$ at the top to $1000T$ at the bottom. The intensity at 0.020 Å^{-1} is in the reverse order, $1000T$ at the top and $200T$ at the bottom

Scattering curves for this simple growth model are nearly self-similar. *Figure 11* shows, for $L_0 = 50$ Å and $L_1 = 10$ Å, the scattering curves for $10T$ and $100T$. In addition, the $10T$ curve multiplied by 10 is also shown, in order to place it at nearly the same intensity level as the $100T$ curve. The $100T$ and the modified $10T$ curves are very similar. The self-similarity improves as curves from longer times are compared, because the early-time shape changes are then gone.

Simulated SAXS curves for the initially thinner cystallites ($L_0 = 20$ Å) and slow thickening ($L_1 = 2$ Å) are shown in *Figure 12*. The principal difference between this case and that for $L_0 = 50$ Å is the presence and growth of a

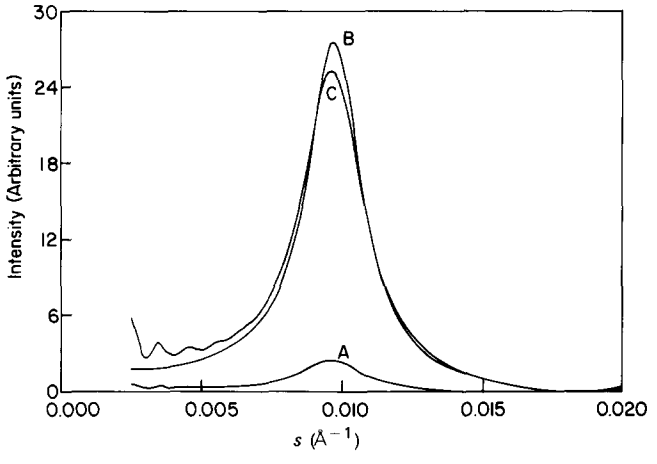

Figure 11 Simulated 'classical growth' scattering curves for $t = 10T$ (curve A), $t = 10T$ but multiplied by 10 (curve B), and $t = 100T$ (curve C)

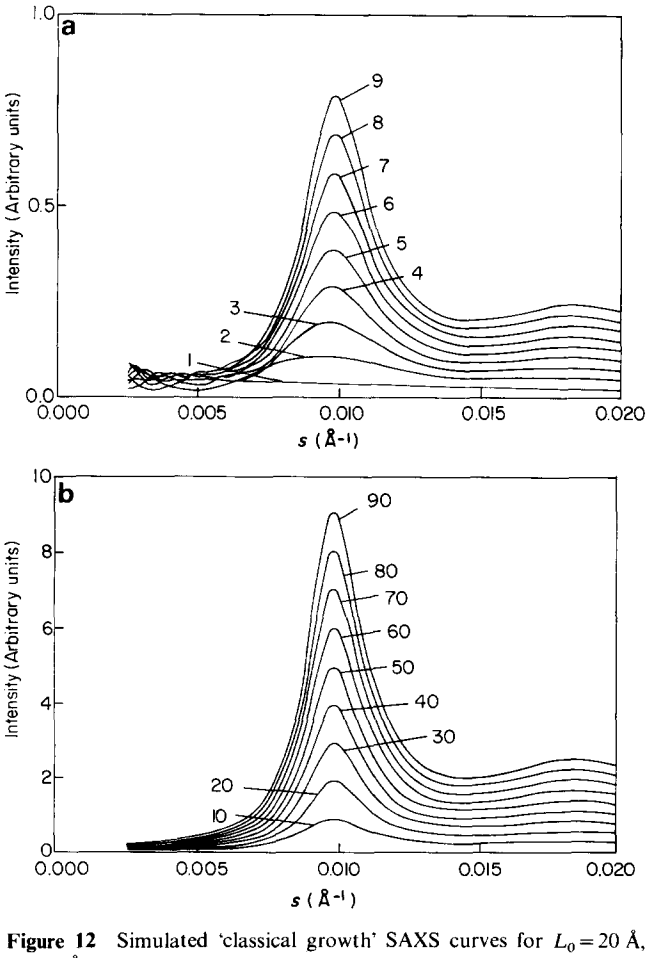

Figure 12 Simulated 'classical growth' SAXS curves for $L_0 = 20$ Å, $L_1 = 2$ Å. Curves are labelled with values of t/T

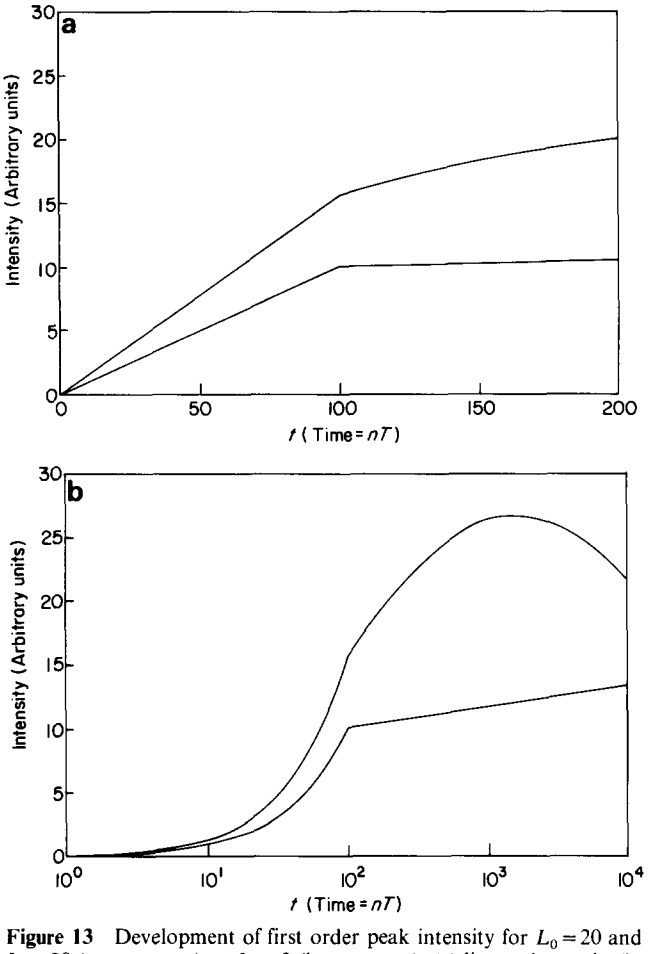

Figure 13 Development of first order peak intensity for $L_0 = 20$ and $L_1 = 20$ (upper curve) or $L_1 = 2$ (lower curve): (a) linear time axis, (b) logarithmic time axis

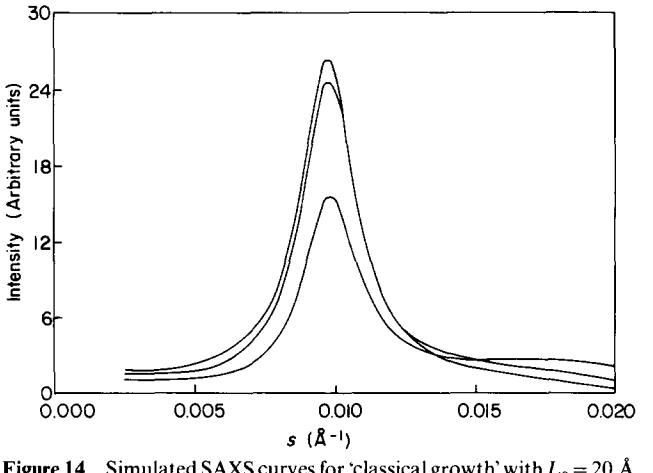

Figure 14 Simulated SAXS curves for 'classical growth' with $L_0 = 20$ Å, $L_1 = 20$ Å, for $t = 100T$ (lowest curve), $t = 500T$ second curve, and $t = 1000T$ (highest curve). The intensity order at $s = 0.02$ Å^{-1} is in the order $1000T$ (lowest) to $100T$ (highest)

second-order maximum. Simulation with $L_0 = 20$ Å, $L_1 = 20$ Å (not shown) is qualitatively similar to that shown in *Figure 12*, except that the second order peak grows somewhat less rapidly.

Figure 13 shows the development of the first-order peak intensity with transformation time for $L_0 = 20$ Å. During stack building ($T \leqslant 100$), the intensity builds essentially linearly, with crystal thickening contributing markedly to the rate of the linear increase. The expected maximum occurs at longer times.

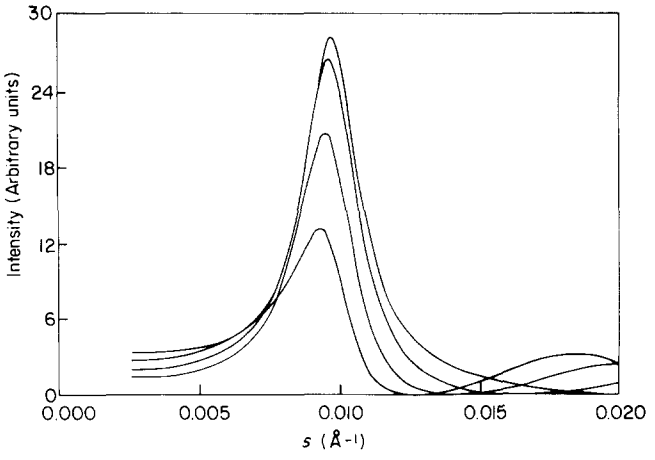

Figure 15 Simulated curves for $L = 100$ Å, $L_1 = 0$ and $L_0 = 50$ Å (highest curve), 60 Å, 70 Å, and 80 Å (lowest curve)

As the transformation progresses for $L_0 = 20$ Å, the crystallites thicken gradually toward $\bar{L}/2$ and the intensity of the second order maximum decreases. This effect is shown in *Figure 14*.

As has been shown in the above examples, for degrees of crystallinity above 50%, with increasing crystallinity the first-order peak decreases in intensity and the second-order peak increases. This is shown explicitly in *Figure 15*, where scattering curves for an average degree of crystallinity of 50%, 60%, 70% and 80% are shown. It is to be noticed also that the first order maximum shifts to slightly smaller angles, correlated with an intensity decrease of the peak.

DISCUSSION

As has been shown above, there are several systematic differences in small-angle scattering curve development between classical growth and spinodal demixing. These differences are summarized below:

Peak position

For classical growth, the first-order SAXS peak shows a gradual movement toward higher angle initially, thereafter remaining substantially constant. In the spinodal case, the peak position is constant at all times.

Peak shape

For classical growth, the first-order peaks are self-similar, once they have attained their constant angular position. In the spinodal case, the peaks are self-similar only after the zero-time peak has been subtracted.

Second-order

For classical growth, intensity at the second-order peak is always observed except when the degree of crystallinity within the stack is 50%. The relative height of the second order peak decreases symmetrically with crystallinity from 0% to 50% and from 100% to 50%. For the spinodal process, no intensity is found at the second-order position.

Intensity cross-over

For the spinodal case, there is an intensity cross-over at some critical angle $2\theta_c$ beyond the peak. For an ideal spinodal, $2\theta_c = \sqrt{2}(2\theta_p)$, where $(2\theta)_p$ is the peak position. For most classical growth behaviour the intensity curves elevate uniformly through all angles and no cross-over is ordinarily to be observed.

Intensity decrease

Only for the case of classical growth can the SAXS peaks decrease in intensity with degree of transformation. This occurs as the crystallinity exceeds 50%.

SUMMARY

The scattering from classical growth transformations with initial stack crystallinities lower than and equal to the critical value of 50% have been simulated and compared. In the former case, the intensity moves smoothly through a maximum. For the latter case, when the rate of crystal thickening is much slower than that of stack growth, the transition from an increasing to a decreasing intensity occurs sharply when stack growth is complete. The presence and rate of change of a second-order maximum depends on the initial stack crystallinity and on the rate of crystal thickening. It is to be a reemphasized that only for 50% crystallinity is there no intensity at the second order position.

ACKNOWLEDGEMENTS

This work was initiated as a term project in MET 801. The authors are grateful to others who participated in the project and contributed to its success: Ute Abbott, Keh-Gong Lee, and Shekhar Wadekar.

REFERENCES

1 Hoffman, J. D. and Weeks, J. J. *J. Chem. Phys.* 1965, **42**, 4301
2 Schultz, J. M., Robinson, W. H. and Pound, G. M. *J. Polym. Sci. A-2* 1967, **5**, 511
3 Oda, T. and Stein, R. S. *J. Polym. Sci. A-2* 1972, **10**, 685
4 Petermann, J. and Schultz, J. M. *J. Mater. Sci.* 1978, **13**, 2188
5 Schultz, J. M. *J. Polym. Sci., Polym. Phys. Edn.* 1976, **14**, 2291
6 Schultz, J. M., Lin, J. S. and Hendricks, R. W. *J. Appl. Cryst.* 1978, **11**, 551
7 Elsner, G., Koch, M. H. J., Bordas, J. and Zachmann, H. G. *Makromol. Chem.* 1981, **182**, 1263
8 Magill, J. M., Lin, J. S. and Schultz, J. M., in preparation
9 Schultz, J. M., Lin, J. S., Hendricks, R. W., Petermann, J. and Gohil, R. M. *J. Polym. Sci., Polym. Phys. Edn.* 1981, **19**, 609
10 Petermann, J., Gohil, R. M., Schultz, J. M., Hendricks, R. W. and Lin, J. S. *J. Polym. Sci., Polym. Phys. Edn.* 1982, **20**, 523
11 Koch, M. J. H., Bordas, J., Schola, E. and Broecker, H. Chr. *Polym. Bull.* 1979, **1**, 709
12 Gupte, K. M., Motz, Heike and Schultz, J. M. *J. Polym. Sci., Polym. Phys. Edn.* 1983, **21**, 1927
13 Peszkin, Perla and Schultz, J. M. *Bull. Am. Phys. Soc.* 1984, **29**, 241
14 Gunther, R.-H. *Ph.D. Dissertation*, Universitat Mainz, 1981
15 Babajko, Suzanne and Schultz, J. M. *J. Polym. Sci., Polym. Phys. Edn.* 1982, **20**, 497
16 Elad, J. and Schultz, J. M. *J. Polym. Sci., Polym. Phys. Edn.* 1984, **22**, 781
17 Petermann, J. *Makromol. Chem.* 1981, **182**, 613
18 Cahn, J. W. *Acta Met.* 1961, **9**, 795
19 Cahn, J. W. *Trans. Met. Soc. AIME* 1968, **242**, 166
20 Swanger, L. A., Gupta, P. K. and Cooper, A. R. Jr. *Acta Met.* 1970, **18**, 9
21 de Fontaine, D. in 'Ultrafine Grain Metals' (Eds. J. H. Burke and V. Weiss), Syracuse University Press, 1970
22 Cook, H. E. Jr. *Acta Met.* 1970, **18**, 297
23 Williams, R. O. *Acta Met.* 1981, **29**, 95

24 Bernauer, F. 'Gedrillte Kristalle' Verlag Gebrüder Borntraeger, Berlin, 1929
25 Geil, P. H. 'Polymer Single Crystals', Wiley–Interscience, New York, 1963
26 Keller, A. *Nature* 1954, **174**, 926
27 Keller, A. *J. Polym. Sci.* 1955, **15**, 31
28 Weeks, J. J. *J. Res. Natl. Bur. Stand.* 1963, **A67**, 441
29 Hoffman, J. D. and Weeks, J. J. *J. Chem. Phys.* 1965, **42**, 4301
30 Peterlin, A. *J. Polym. Sci.* 1963, **1B**, 279
31 Kavesh, S. and Schultz, J. M. *J. Polym. Sci. A-2* 1971, **9**
32 Fischer, O., Rennie, A. R., Schultz, J. M., Zietz, R. and Fischer, E. W., to be published
33 Peszkin, P. N. *Ph.D. Dissertation*, University of Delaware, 1984
34 Hosemann, R. and Bagchi, S. N. in 'Direct Analysis of Diffraction by Matter', North-Holland, Amsterdam, 1962
35 Guinier, A. 'Théorie et Technique de la Radiocristallographie', Dunod, Paris, 1956